Probing the nature of dark matter through the metal enrichment of the intergalactic medium

Bremer, Jonas; Dayal, Pratika; Ryan-Weber, Emma V.

Published in:
Monthly Notices of the Royal Astronomical Society

DOI:
10.1093/mnras/sty771

Monthly Notices
of the
ROYAL ASTRONOMICAL SOCIETY

MNRAS **477,** 2154–2163 (2018)
Advance Access publication 2018 March 23

doi:10.1093/mnras/sty771

Probing the nature of dark matter through the metal enrichment of the intergalactic medium

Jonas Bremer,[1]★ Pratika Dayal[1] and Emma V. Ryan-Weber[2]

[1]*Kapteyn Astronomical Institute, University of Groningen, PO Box 800, NL-9700 AV Groningen, the Netherlands*
[2]*Centre for Astrophysics and Supercomputing, Swinburne University of Technology, PO Box 218, Hawthorn, VIC 3122, Australia*

Accepted 2018 March 19. Received 2018 March 12; in original form 2017 September 22

ABSTRACT

We focus on exploring the metal enrichment of the intergalactic medium (IGM) in cold and warm (1.5 and 3 keV) dark matter (DM) cosmologies, and the constraints this yields on the DM particle mass, using a semi-analytic model, DELPHI, that jointly tracks the DM and baryonic assembly of galaxies at $z \simeq 4$–20 including both supernova (SN) and (a range of) reionization feedback (models). We find that while $M_{\rm UV} \gtrsim -15$ galaxies contribute half of all IGM metals in the cold dark matter (CDM) model by $z \simeq 4.5$, given the suppression of low-mass haloes, larger haloes with $M_{\rm UV} \lesssim -15$ provide about 80 per cent of the IGM metal budget in 1.5 keV warm dark matter (WDM) models using two different models for the metallicity of the interstellar medium. Our results also show that the only models compatible with two different high-redshift data sets, provided by the evolving ultraviolet luminosity function (UV LF) at $z \simeq 6$–10 and IGM metal density, are standard CDM and 3 keV WDM that do not include any reionization feedback; a combination of the UV LF and the Díaz et al. point provides a weaker constraint, allowing CDM and 3 and 1.5 keV WDM models with SN feedback only, as well as CDM with complete gas suppression of all haloes with $v_{\rm circ} \lesssim 30\,{\rm km\,s^{-1}}$. Tightening the error bars on the IGM metal enrichment, future observations, at $z \gtrsim 5.5$, could therefore represent an alternative way of shedding light on the nature of DM.

Key words: galaxies: evolution – galaxies: high-redshift – intergalactic medium – dark matter.

1 INTRODUCTION

The particle nature of dark matter (DM) remains one of the key outstanding problems in the field of physical cosmology. The standard Lambda cold dark matter (ΛCDM) cosmological model has now been successfully tested using the large-scale (10–100 Mpc) structure of the Universe inferred from the cosmic microwave background (CMB), the Lyman-α forest, galaxy clustering, and weak lensing (see e.g. Weinberg et al. 2015). However, the elegance of this picture is marred by the fact that CDM seems to exhibit an excess of power on small scales (summarized in e.g. Weinberg et al. 2015; Del Popolo & Le Delliou 2017). This 'small-scale crisis' manifests itself in the observed lack of theoretically predicted satellites of the Milky Way ('the missing satellite problem'; Klypin et al. 1999; Moore et al. 1999b), DM haloes being too dense as compared to observations ('the core-cusp problem'; Navarro, Frenk & White 1997; Moore et al. 1999a), and in the lack of theoretically predicted massive satellites of the Milky Way ('too big to fail problem'; Boylan-Kolchin, Bullock & Kaplinghat 2011, 2012). Although some of these problems can be solved purely through the effects of baryonic feedback including, but not limited to, the effects of supernovae (SN) and parent–satellite interactions (Koposov et al. 2009; Governato et al. 2012, 2015; Macciò et al. 2012a; Peñarrubia et al. 2012; Garrison-Kimmel et al. 2013; Del Popolo & Le Delliou 2014; Di Cintio et al. 2014; Madau, Shen & Governato 2014; Silk 2017), an alternative route focuses on questioning the cold nature of DM itself. One such alternative candidate is provided by warm dark matter (WDM) with particle masses $m_x \sim \mathcal{O}$(keV) (e.g. Bode, Ostriker & Turok 2001). In addition to its particle-physics motivated nature, the WDM model has been lent support by the observations of a 3.5 keV line from the Perseus cluster that might arise from the annihilation of light sterile neutrinos into photons (Boyarsky et al. 2014; Bulbul et al. 2014; Cappelluti et al. 2018). However, other works (Macciò et al. 2012b; Schneider et al. 2014) caution that the power suppression arising from WDM makes it incompatible with observations, leaving the field open to other models including fuzzy CDM consisting of ultra-light $\mathcal{O}(10^{-22}\,{\rm eV})$ boson or scalar particles (Hu, Barkana & Gruzinov 2000; Du, Behrens & Niemeyer 2017; Hui et al. 2017), self-interacting DM (Spergel & Steinhardt 2000; Rocha et al. 2013; Vogelsberger et al. 2014), and decaying DM (Wang et al. 2014). The most recent estimates of the (thermally decoupled) WDM particle mass range between $m_x \gtrsim 2$–2.9 keV (using Milky Way dwarf satellites; Kennedy et al.

★ E-mail: bremer@astro.rug.nl

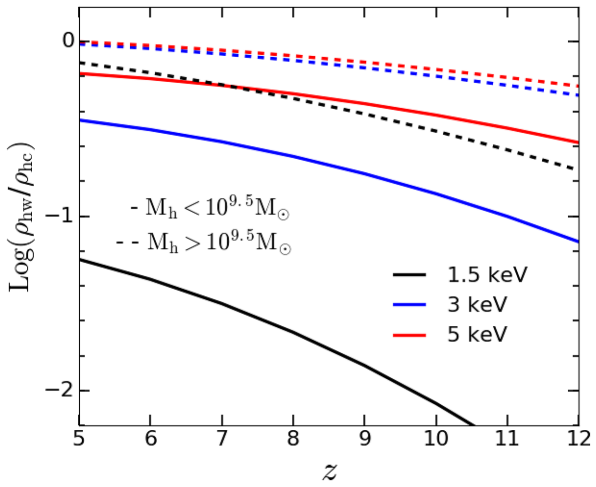

Figure 1. As a function of redshift, we show the (log) cumulative mass density bound in WDM haloes ($\rho_{\rm hw}$) relative to CDM ($\rho_{\rm hc}$) for three different WDM masses: 1.5 keV (black lines), 3 keV (blue lines), and 5 keV (red lines), respectively. Solid and dashed lines show the mass bound in haloes with $M_{\rm h} \lesssim 10^{9.5}\,{\rm M}_\odot$ and $M_{\rm h} \gtrsim 10^{9.5}\,{\rm M}_\odot$, respectively.

2014; Jethwa, Erkal & Belokurov 2018), $m_x \gtrsim 2.9-5.3$ keV (from Lyman-α forest statistics; Viel et al. 2013; Baur et al. 2016; Iršič et al. 2017), $m_x \gtrsim 1.3-3$ keV (from reionization; Tan, Wang & Cheng 2016; Lopez-Honorez et al. 2017), $m_x > 1.8$ keV (from ultra-deep ultraviolet luminosity functions at $z \simeq 2$; Menci et al. 2016a), $m_x \gtrsim 1.6$ keV (from high-z gamma-ray bursts; de Souza et al. 2013), and $m_x \gtrsim 1-2.1$ keV (by modelling high-z galaxies and gravitational lenses; Pacucci, Mesinger & Haiman 2013; Inoue et al. 2015; Menci et al. 2016b; Birrer, Amara & Refregier 2017). A number of works have also shown how forthcoming observations with, for example, the *James Webb Space Telescope* (*JWST*) can be used to differentiate between $m_x \lesssim 1.5$ keV and $m_x \gtrsim 3$ keV WDM using the redshift-dependent growth of the stellar mass density (SMD; Dayal, Mesinger & Pacucci 2015), stellar mass–halo mass relations (Dayal et al. 2017a), and high-z direct collapse black holes (Dayal et al. 2017b).

In this *proof-of-concept* work, our aim is to, first, study the metal enrichment of the intergalactic medium (IGM) at high z ($z \gtrsim 4$) in both cold and warm matter cosmologies and, secondly, check if the IGM metal enrichment can be used to place constraints on the WDM particle mass. Our motivation arises from the fact that, with their shallow potentials, galaxies with low halo masses ($\lesssim 10^{9.5}\,{\rm M}_\odot$) are expected to be the dominant contributors to the IGM metal budget at high z (e.g. Oppenheimer, Davé & Finlator 2009; Shen et al. 2013; Díaz et al. 2015; Finlator et al. 2015; García et al. 2017a). Therefore, the increasing lack of such low-mass haloes, due to an increasing suppression of small-scale power, with decreasing m_x will lead to both a delay and a decrease in the IGM metal enrichment at early cosmic epochs.

We illustrate this point using Fig. 1 that shows the cumulative mass density contained in bound DM haloes in three different WDM models, with $m_x = 1.5$, 3, and 5 keV, with respect to CDM. First, focusing at $M_{\rm h} \gtrsim 10^{9.5}\,{\rm M}_\odot$ haloes, we see that the 5 keV WDM particle is heavy enough to have assembled 55 per cent of the total mass density of CDM haloes by $z \simeq 12$, increasing to $\sim$100 per cent by $z \simeq 5$. Given its low mass, and correspondingly large suppression of power on small scales, the 1.5 keV WDM model has only assembled about 18 per cent of the halo mass density compared to CDM by $z \simeq 12$, increasing to $\sim$76 per cent by $z \simeq 5$; as expected, the 3 keV model straddles the range between these two extremes, lying close to the 5 keV WDM results. On the other hand, there is significant bound DM mass missing when considering low-mass haloes with $M_{\rm h} \lesssim 10^{9.5}\,{\rm M}_\odot$: indeed, the 1.5 keV WDM model assembles <1 per cent of the total CDM mass in such haloes at $z \simeq 12$, rising only to $\sim$6 per cent by $z \simeq 5$. This dearth of bound haloes naturally implies a dearth in metal production and, by extension, the metal enrichment of the IGM. As expected, the bound mass fraction increases with m_x to $\sim$26 per cent at $z \simeq 12$ and is as high as 66 per cent at $z \simeq 5$ for 5 keV WDM.

We start by describing the theoretical model in Section 2. We quantify the impact of both SN feedback and (a suite of) reionization feedback scenarios on, both, the stellar/gas content of early galaxies in Section 3 before evaluating the metal enrichment of the IGM and comparing to the observed IGM metallicities in Section 4. Throughout this paper, we use the latest cosmological parameters as measured by the *Planck* satellite (Planck Collaboration XIII 2016) such that $(\Omega_{\rm m}, \Omega_\Lambda, \Omega_{\rm b}, h, n_{\rm s}, \sigma_8) = (0.3089, 0.6911, 0.0486, 0.6774, 0.9667, 0.8159)$ and quote all quantities in comoving units unless stated otherwise. Here, $\Omega_{\rm m}, \Omega_\Lambda, \Omega_{\rm b}$ represent the density parameters for matter, dark energy, and baryons, respectively, h is the Hubble value, $n_{\rm s}$ is the spectral index of the initial density perturbations, and σ_8 represents the root-mean-square density fluctuations on scales of $8h^{-1}$ cMpc.

2 THE THEORETICAL MODEL

The calculations presented in this work are based on the semi-analytic model DELPHI (**D**ark Matter and the **e**mergence of ga**l**axies in the e**p**oc**h** of re**i**onization; Dayal et al. 2014, 2015, 2017a,b) that jointly tracks the DM and baryonic assembly of high-z ($z \sim$ 4–20) galaxies. We start by generating modified binary merger trees with accretion (Parkinson, Cole & Helly 2008) for 800 (4000) galaxies at $z = 4$ in CDM (1.5 keV WDM), uniformly distributed in the halo mass range $\log(M_{\rm h}/{\rm M}_\odot) = 9-13$. We use the modifications required to generate merger trees for WDM presented in Benson et al. (2013) that include (a) introducing an m_x-dependent cut-off in the initial power spectrum; (b) using an m_x-dependent critical overdensity of collapse; (c) using a sharp window function in k-space; and (d) using numerically calibrated DM infall rates. Matching to the Sheth–Tormen halo mass function (HMF) at $z = 4$ yields the (comoving) number density for each halo that is propagated throughout its merger tree; we have confirmed that the resulting HMFs are in agreement with the Sheth–Tormen HMF at all $z \simeq 4.5$–20.

As for the baryonic physics, the first progenitor(s) of any halo are assigned a gas mass that scales with the halo mass through the cosmological ratio such that $M_{\rm g} = (\Omega_{\rm b}/\Omega_{\rm m})M_{\rm h}$. A fraction of this gas mass is converted into stars with an effective star formation efficiency ($f_*^{\rm eff}$) that is the minimum between the efficiency that produces enough Type II supernova (SNII) energy to eject the rest of the gas, $f_*^{\rm ej}$, and an upper maximum threshold, f_*, so that $f_*^{\rm eff} = \min[f_*^{\rm ej}, f_*]$. We calculate the newly formed stellar mass at any z as $M_*(z) = M_{\rm g}(z) f_*^{\rm eff}$ and the final gas mass at the end of the z-step, including that lost in star formation and SN feedback, is then given by $M_{\rm gf}(z) = [M_{\rm g}(z) - M_*(z)][1 - (f_*^{\rm eff}/f_*^{\rm ej})]$. At each z-step, we also account for DM that is smoothly accreted from the IGM, making the reasonable assumption that this is accompanied by accretion of a cosmological fraction $(\Omega_{\rm b}/\Omega_{\rm m})$ of gas mass.

We use a Salpeter initial mass function (IMF; Salpeter 1955) between 0.1 and 100 ${\rm M}_\odot$ throughout this work. Assuming a fixed metallicity of $0.2\,{\rm Z}_\odot$ for all stars, we then use the stellar

population synthesis code STARBURST99 (Leitherer et al. 1999, 2010) to generate the complete spectrum for each galaxy summing over all its entire star formation history. This physical prescription yields model results in excellent agreement with all currently available data sets for high-z ($z \gtrsim 5$) galaxies, from the evolving ultraviolet luminosity function (UV LF) to the SMD to mass-to-light ratios to the z-evolution of the stellar mass and UV luminosity densities, for both CDM and WDM. We note that the model only uses two mass- and z-independent free parameters: to match to observations, we require (roughly) 10 per cent of the SNII energy coupling to the gas ($f_{\rm w}$) and a maximum (instantaneous) star formation efficiency of $f_* = 3.5$ per cent. This (SNII feedback only) model is designated as the *fiducial model* in what follows.

In this work, we also include the effects of the ultraviolet background (UVB) created during reionization, which, by heating the ionized IGM to $T \sim 10^4$ K, can have an impact on the baryonic content of low-mass haloes (e.g. Okamoto, Gao & Theuns 2008; Petkova & Springel 2011; Ocvirk et al. 2016). Maintaining the same SNII feedback and f_* parameters as the fiducial model, in this work, we also consider three (maximal) UVB-feedback scenarios in which the gas mass is completely photoevaporated for haloes: (i) below a characteristic halo mass of $M_{\rm h} = 10^9\,{\rm M}_\odot$; (ii) below a circular velocity of $v_{\rm circ} = 30\,{\rm km\,s^{-1}}$; and (iii) below a circular velocity of $v_{\rm circ} = 50\,{\rm km\,s^{-1}}$. In the latter two cases, the minimum halo mass affected by the UVB increases with decreasing z [since $v_{\rm circ}(z) \propto M_{\rm h}^{0.33}(1+z)^{0.5}$] from $M_{\rm h} \simeq 10^{8.6}$ to $M_{\rm h} \simeq 10^{9.1}\,{\rm M}_\odot$ ($\simeq 10^{9.2}$ to $10^{9.7}\,{\rm M}_\odot$) from $z \simeq 12$ to 5 for a velocity cut of $v_{\rm circ} = 30\,{\rm km\,s^{-1}}$ ($50\,{\rm km\,s^{-1}}$). Therefore, the UV feedback scenario with $M_{\rm h} = 10^9\,{\rm M}_\odot$ lies between the constant velocity cut-off cases considered here, lying close to case (iii) at the highest redshifts and slowly tending towards case (ii) by $z \simeq 5$.

Finally, in order to calculate the IGM metal enrichment driven by outflows from these early galaxy populations, we assume gas and metals to be perfectly mixed in the interstellar medium (ISM), and carry out calculations for two limiting scenarios: the first, where every galaxy has a fixed metallicity of $Z_{\rm gas} = 0.20\,{\rm Z}_\odot$ and the second where the gas-phase metallicity for each galaxy depends on its stellar mass.

3 IMPACT OF FEEDBACK IN CDM AND WDM MODELS

We now use the model explained above to quantify the impact of internal (SNII) and external (UVB) feedback on galaxy observables, including the evolving UV LF and the SMD, and intrinsic properties, such as the total density of ejected gas mass, for both CDM and WDM cosmologies.

3.1 Feedback impact on the UV LF

Quantifying the number density of Lyman break galaxies (LBG) as a function of the UV luminosity, the UV LF, and its z-evolution offers a robust data set against which to calibrate the model. As noted above, DELPHI uses two parameters to match to the observed data – an instantaneous star formation efficiency ($f_* = 0.035$) and the fraction of SNII energy coupling to gas ($f_{\rm w} = 0.1$) that, broadly, impact the bright and faint ends of the UV LF, respectively. The results of these calculations are shown in Fig. 2. Starting with CDM, the fiducial model extends to magnitudes as faint as $M_{\rm UV} = -10\,(-12)$ for $z \simeq 5\,(12)$ with a faint-end slope that evolves as $\alpha = -1.75\log(z) - 0.52$ (see also Dayal et al. 2014). We note that this model is in excellent agreement with all available observational data at $z \simeq 6$–10; the slight overprediction of the number density of the rarest brightest $z \simeq 6$ galaxies possibly arises due to our ignoring the effects of dust attenuation for these massive systems. Given that the impact of UV feedback, in suppressing the baryonic content of low-mass haloes, progressively increases using a cut-off of $v_{\rm circ} = 30\,{\rm km\,s^{-1}}$ to $M_{\rm h} = 10^9\,{\rm M}_\odot$ to $v_{\rm circ} = 50\,{\rm km\,s^{-1}}$, we find that the UV LF starts peeling away from the fiducial UV LF at increasing luminosities (decreasing magnitudes) in the same order. Indeed, as seen from Fig. 2, cutting off at $M_{\rm UV} \sim -12.5$ at $z \simeq 6$, the CDM UV feedback models assuming no gas in haloes below $M_{\rm h} = 10^9\,{\rm M}_\odot$ and $v_{\rm circ} = 30\,{\rm km\,s^{-1}}$ are compatible with all available observations except for the faintest $M_{\rm UV} = -12.5$ point at $z \simeq 6$ inferred using lensed *Hubble Space telescope* data (Livermore et al. 2017). A confirmation of the faint-end slope persistently rising to such faint magnitudes, corresponding to halo masses of about $10^{8.5-9}\,{\rm M}_\odot$, might be a powerful test of the nature of DM and the impact of feedback on these low-mass systems. However, with its impact on larger halo masses, the $v_{\rm circ} = 50\,{\rm km\,s^{-1}}$ model naturally cuts off at higher luminosities corresponding to $M_{\rm UV} \approx -15\,(-16)$ at $z \simeq 6\,(12)$ – using current data, we can therefore rule out this maximal UV suppression model. We also find that, although, the halo mass range affected by UV feedback increases by about 0.5 dex between $z \simeq 13$ and 5, the shift in the UV LF between this range is larger ($\sim$1.5 mag) than the expected value ($\sim$0.75) – this is the result of the $L_{\rm UV}/M_*$ value decreasing with decreasing z (see fig. 7; Dayal et al. 2014). Yielding results in accord with CDM down to $M_{\rm UV} \approx -11\,(-13)$ at $z \simeq 6\,(12)$, the fiducial 3 keV WDM model is in accord with all available data points; indeed, the 3 keV WDM for complete UV suppression in all haloes below $v_{\rm circ} = 30\,{\rm km\,s^{-1}}$ also matches all available data except the faintest $M_{\rm UV} = -12.5$ point at $z \simeq 6$ (Livermore et al. 2017).

The 1.5 keV fiducial model yields results that are qualitatively the same as the fiducial CDM case down to $M_{\rm UV} \simeq -13$ at $z \simeq 6$ and, given the increasing lack of low-mass haloes with increasing redshift, turns over at progressively brighter magnitudes with increasing redshift ($M_{\rm UV} \simeq -18$ at $z \simeq 12$). It is interesting to see that the fiducial 1.5 keV model lies close to the CDM $v_{\rm circ} = 50\,{\rm km\,s^{-1}}$ UV feedback case at $z \simeq 12$, and shifts closer to the CDM $v_{\rm circ} = 30\,{\rm km\,s^{-1}}$ case by $z \simeq 6$. We also find that, within error bars, the 1.5 keV fiducial model is also in agreement with all available data except for the one $z = 6$ data point at $M_{\rm UV} = -12.5$ (Livermore et al. 2017). Including the impact of UV feedback, we again find the same trends as CDM, although the magnitude cuts at which the UV LF starts peeling away from the fiducial case correspond to much brighter galaxies. Indeed, unless we modify the baryonic physics for each UV feedback model, we find that current $M_{\rm UV} \gtrsim -14$ LBG data at $z = 6$–7 (Bouwens et al. 2017; Livermore et al. 2017) can effectively be used to rule out 'maximal' UV feedback scenarios. However, we caution that, in principle, only the fraction $(1 - Q_{\rm II}$, where $Q_{\rm II}$ is the volume filling factor of ionized hydrogen) of galaxies embedded in ionized regions should be affected by UV feedback at any redshift. This implies that the 'true' (SNII + UV feedback affected) UV LF should lie between the fiducial and 'maximal' UV suppression cases considered here.

3.2 Feedback impact on the SMD

Encoding the total mass locked up in stars, the SMD, and its redshift evolution presents a crucial test for any model of galaxy formation. Once that our model free parameters have been fixed by matching to the UV LF as explained above, we study the SMD and compare our

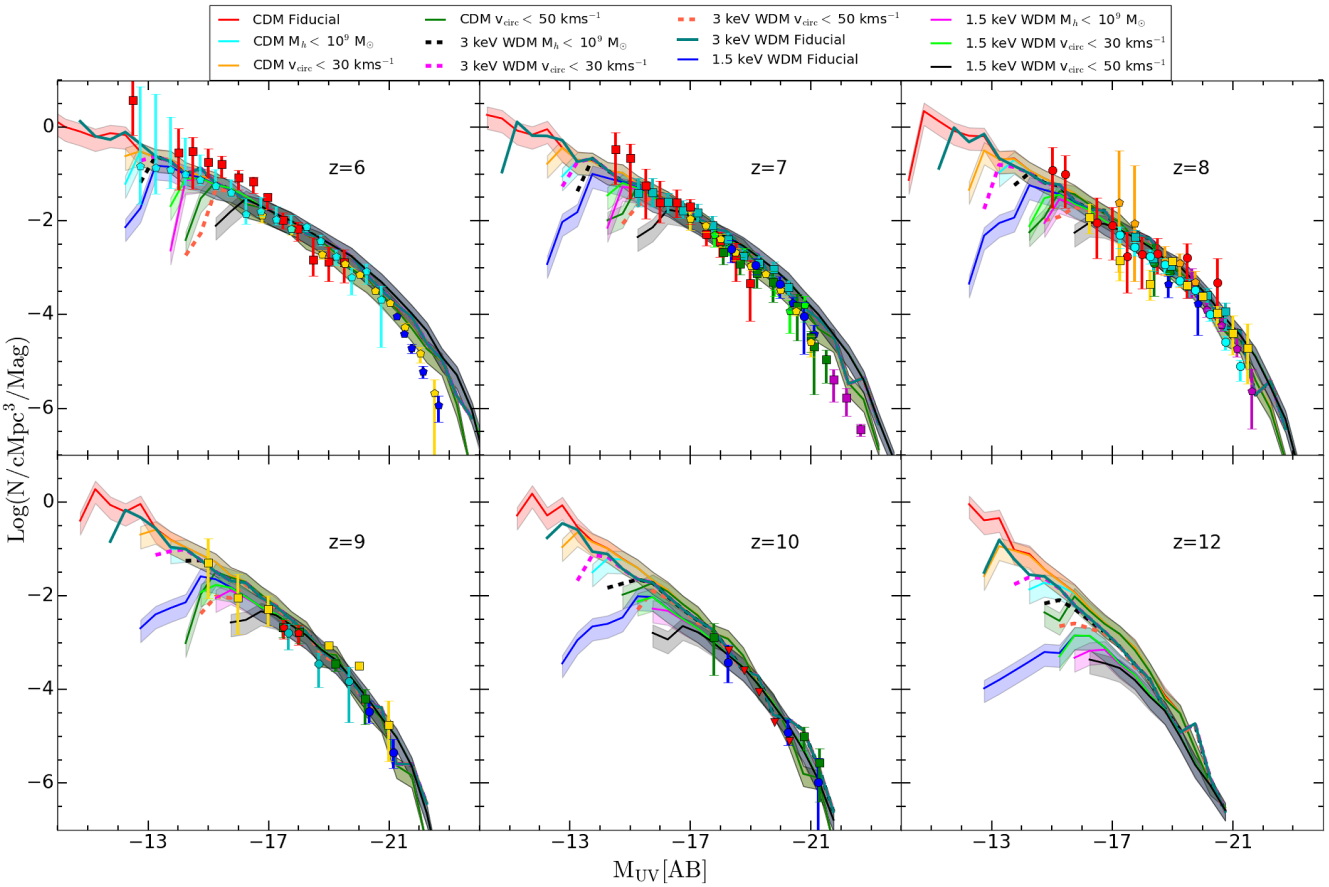

Figure 2. The UV LFs for CDM, 3 and 1.5 keV WDM for $z \simeq 6$–12, as marked. In each panel, the different lines show results for the four feedback models adopted (see Section 2), as marked in the legend, with the shaded regions showing the 1σ Poissonian errors; for clarity, the 3 keV model is shown without errors. In each panel, points show observational data – $z \simeq 6$: Bouwens et al. (2015, gold pentagons), Bowler et al. (2015, blue pentagons), Livermore, Finkelstein & Lotz (2017, red squares), and Bouwens et al. (2017, cyan pentagons); $z \simeq 7$: Castellano et al. (2010, blue pentagons), McLure et al. (2010, green squares), Oesch et al. (2010, blue circles), Bouwens et al. (2011, green pentagons), McLure et al. (2013, gold pentagons), Bowler et al. (2014, magenta squares), Atek et al. (2015, cyan squares), and Livermore et al. (2017, red squares); $z \simeq 8$: Bouwens et al. (2010, green circles), McLure et al. (2010, blue pentagons), Bouwens et al. (2011, cyan squares), Bradley et al. (2012, magenta pentagons), McLure et al. (2013, cyan circles), Atek et al. (2015, orange pentagons), Livermore et al. (2017, red circles), and Ishigaki et al. (2018, gold squares); $z \simeq 9$: McLure et al. (2013, red pentagons), Oesch et al. (2013, cyan hexagons), McLeod, McLure & Dunlop (2016, green squares), Bouwens et al. (2016, blue circles), and Ishigaki et al. (2018, gold squares); $z \simeq 10$: Bouwens et al. (2015, blue circles), Oesch et al. (2014, green squares), and Oesch et al. (2014, red triangles showing the upper limits).

theoretical SMD values with observational data. We start by noting that all CDM and 1.5 keV WDM models, both fiducial and including maximal UV feedback, yield SMD results in excellent agreement with observations of $M_{\rm UV} \lesssim -18$ galaxies. Although a robust test of our model, this implies that currently observed galaxies cannot be used to distinguish between CDM and WDM models, requiring observations to extend down to fainter magnitudes (see also Dayal et al. 2014). In what follows, we limit ourselves to studying CDM and 1.5 keV WDM (corresponding to a sterile neutrino mass of 7.6 keV; Viel et al. 2005) given that their comparison should show the largest dearth of haloes and hence the largest difference in the SMD.

Starting with CDM, we find that the SMD smoothly grows with decreasing redshift as a larger number of galaxies assemble their stellar mass in a given volume. For the fiducial case, the SMD value grows by about two orders of magnitude ($10^{5.75-7.5}\,{\rm M}_\odot\,{\rm Mpc}^{-3}$) over the 800 Myr between $z \simeq 13$ and 5 as shown in Fig. 3. The SMD value decreases with the addition of UV feedback at all z as the baryonic content of low-mass galaxies is progressively suppressed; again, the impact successively increases from a cut-off of $v_{\rm circ} = 30\,{\rm km\,s^{-1}}$ to $M_{\rm h} = 10^9\,{\rm M}_\odot$ to $v_{\rm circ} = 50\,{\rm km\,s^{-1}}$. With decreasing redshift, larger systems assemble for which most of the stellar mass is built up by a combination of *in situ* star formation and mergers of progenitors above the UV suppression mass. This naturally results in a steeper z-evolution of the SMD with increasing UV feedback – indeed, compared to the fiducial case, galaxies in the 'maximal' UV feedback scenario with $v_{\rm circ} = 50\,{\rm km\,s^{-1}}$ assemble only about 11 per cent of the SMD at $z \simeq 13$, which rises to ∼66 per cent by $z \simeq 5$. Both the value of the SMD and the impact of UV feedback decrease when only considering galaxies brighter than a limit of $M_{\rm UV} = -15$, which provide roughly 30 per cent of the SMD at $z \simeq 13$ in the fiducial model rising to about 78 per cent by $z \simeq 5$. As expected, $M_{\rm UV} \lesssim -18$ galaxies that contribute ∼1 per cent (46 per cent) to the total SMD at $z \simeq 13$ (5) are impervious to the effects of UV feedback.

The 1.5 keV WDM model shows a much steeper z-evolution of the SMD compared to CDM, irrespective of the feedback prescription used for the latter, which is the result of two effects: an intrinsic dearth of low-mass haloes and a faster baryonic assembly since WDM galaxies start from larger progenitors that are less feedback

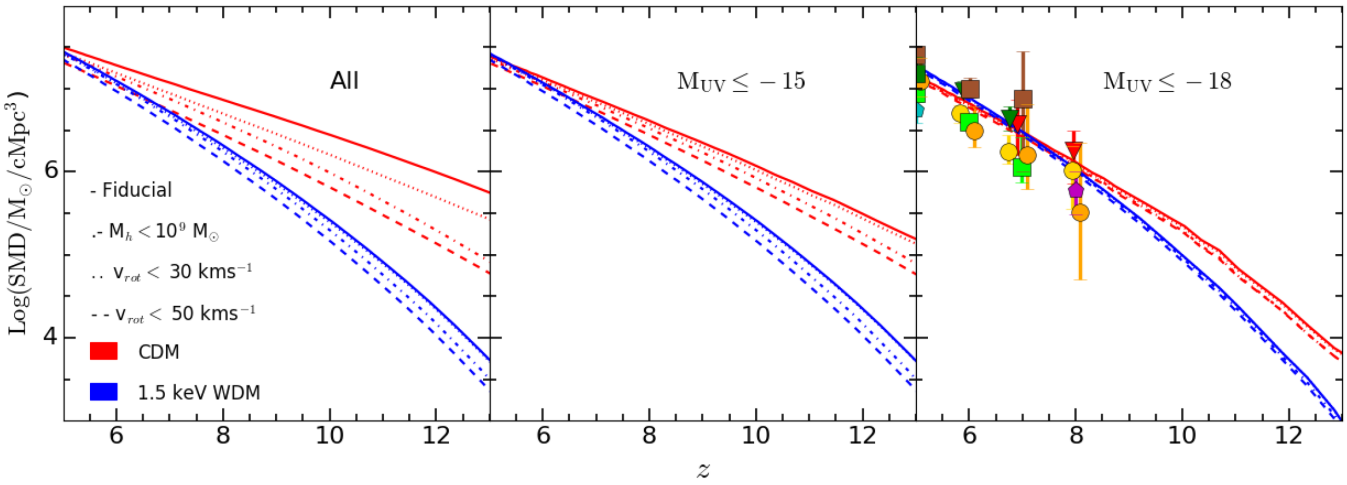

Figure 3. The SMD as a function of redshift for all galaxies (left-hand panel), galaxies with $M_{UV} \lesssim -15$ (middle panel), and $M_{UV} \lesssim -18$ (right-hand panel). In each panel, the red and blue lines show results for CDM and 1.5 keV WDM, respectively, for the different feedback models noted in the legend. Points show SMD measurements inferred using observations for a limiting magnitude of $M_{UV} \simeq -18$: Yabe et al. (2009, green square), Labbé et al. (2010a,b, red triangles), González et al. (2011, green triangles), Lee et al. (2012, cyan pentagon), Labbé et al. (2013, magenta pentagon), Stark et al. (2013, yellow circles), Duncan et al. (2014, brown squares), Grazian et al. (2015, light green squares), and Song et al. (2016, orange circles).

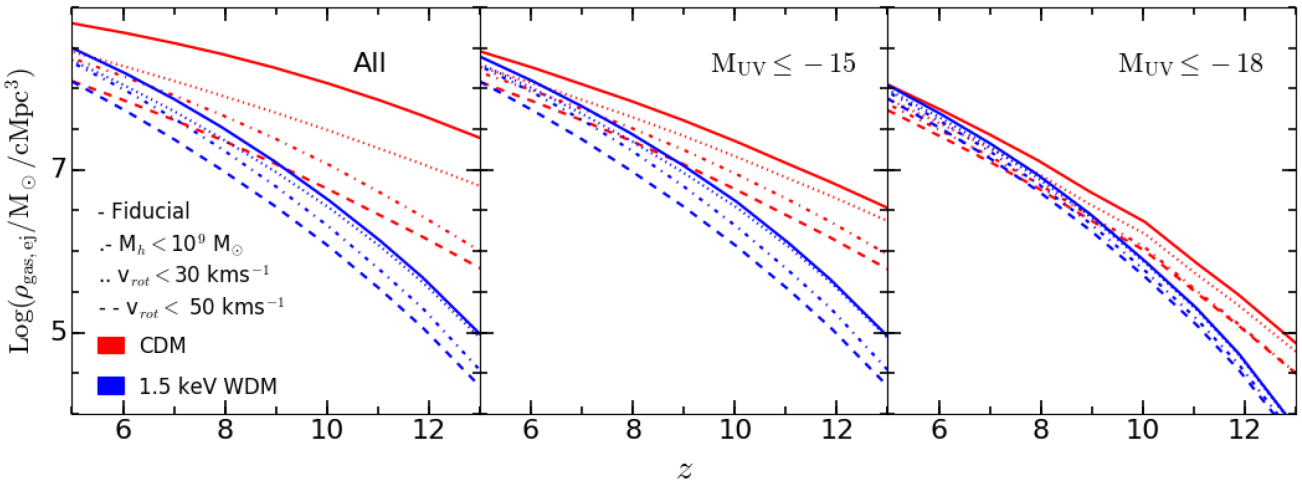

Figure 4. The ejected gas mass density as a function of redshift considering all galaxies (left-hand panel), those with $M_{UV} \lesssim -15$ (middle panel), and $M_{UV} \lesssim -18$ (right-hand panel). In each panel, the red and blue lines show results for CDM and 1.5 keV WDM, respectively, for the different feedback models noted in the legend.

limited (see also Dayal et al. 2014). Indeed, comparing fiducial models, all the galaxies in the 1.5 keV WDM model contain less than 1 per cent of the total SMD at $z \simeq 13$ compared to CDM, thereafter rising steeply to the CDM value at $z \simeq 5$. As expected, the gap between CDM and 1.5 keV WDM SMDs decreases as we consider progressively massive systems with $M_{UV} \lesssim -15$ and as bright as $M_{UV} \lesssim -18$. It is interesting to note that, given its lack of low-mass haloes, the 1.5 keV WDM model is much less affected by UV feedback – the difference between the fiducial and maximal UV feedback models is almost constant at $\lesssim 0.3$ dex compared to the $\sim$1 dex seen for CDM for $M_{UV} \gtrsim -15$ galaxies.

We reiterate the result found in Dayal et al. (2014) – that the z-evolution of the SMD is steeper in the 1.5 keV WDM model, irrespective of the baryonic feedback model considered. The z-evolution of the SMD, integrating down to magnitudes as faint as -16.5 with the *JWST*, can therefore be a powerful probe of the nature of DM.

3.3 Feedback impact on the ejected gas mass density

Now that our model results, for both CDM and 1.5 keV WDM, have been shown to match existing observations, we study the impact of feedback on the total ejected gas mass density integrated over the entire history of all galaxies – $\rho_{gas,ej}$ (Fig. 4). Given our assumption of perfect metal mixing in the ISM, $\rho_{gas,ej}$ is an excellent tracer of the metal enrichment of the IGM, as discussed in Section 4 that follows.

Starting by considering all galaxies in CDM, we find that $\rho_{gas,ej}$ in the fiducial case is about 44 (20) times higher than the SMD at $z \simeq 13$ (5) indicating the enormous impact of SNII feedback in ejecting gas from the potential wells of low-mass haloes. As in the SMD studied above, the complete suppression of baryonic mass leads to a decrease in the ejected gas mass density when using a cut-off of $v_{circ} = 30\,km\,s^{-1}$ to $M_h = 10^9\,M_\odot$ to $v_{circ} = 50\,km\,s^{-1}$. Using a UV feedback cut-off value of $M_h = 10^9\,M_\odot$ ($v_{circ} = 50\,km\,s^{-1}$) results in $\rho_{gas,ej}$ decreasing by a factor of 40 (25) at $z \simeq 13$, reducing

to a factor of 3 (5) by $z \simeq 5$. As expected, the value of $\rho_{\rm gas,\,ej}$ progressively decreases when considering galaxies with $M_{\rm UV} \lesssim -15$ and $M_{\rm UV} \lesssim -18$. Comparing values in the fiducial models, galaxies brighter than a magnitude limit of $M_{\rm UV} \lesssim -15\,(-18)$ only contribute about 13 (0.2) per cent to the total $\rho_{\rm gas,\,ej}$ value at $z \simeq 13$ that rises to about 45 (18) per cent by $z \simeq 5$, implying that the most ejected gas mass comes from galaxies fainter than $M_{\rm UV} = -15$ in CDM. Naturally, given the suppression of the baryonic component of low-mass haloes, including UV feedback results in a smaller difference when comparing $\rho_{\rm gas,\,ej}$ from all galaxies to those above a certain magnitude cut. We also note that the difference between $\rho_{\rm gas,\,ej}$ values for the fiducial and UV feedback models decreases when only considering relatively bright galaxies from about 1.6 dex for all galaxies to about 0.8 (0.4) dex for $M_{\rm UV} \lesssim -15\,(-18)$ at $z \simeq 13$.

As for the 1.5 keV WDM, a dearth of low-mass haloes leads to a lower $\rho_{\rm gas,\,ej}$ value compared with CDM in any feedback scenario at $z \gtrsim 9$ with most (∼79 per cent) of the ejected gas mass density now being contributed by galaxies brighter than $M_{\rm UV} = -15$ at $z \approx 5$. Further, the $\rho_{\rm gas,\,ej}$ trend flips at lower z with 1.5 keV WDM models that include UV feedback having a larger ejected gas mass density value compared to the corresponding CDM model. Analogous to the steeper build-up of the SMD discussed above, this is a result of galaxies starting from larger, and hence less feedback-limited, progenitors in 1.5 keV WDM that have higher star formation rates leading to a larger ejection of gas mass at later epochs. As also noted for the SMD, we see that the difference between the fiducial and UV feedback-limited $\rho_{\rm gas,\,ej}$ values is roughly constant at ∼0.5 dex, compared to the larger and z-dependent values seen for CDM, with the differences being of the order of 0.2 dex for a magnitude cut of $M_{\rm UV} \lesssim -18$. Finally, we note that the relative CDM and 1.5 keV trends discussed here imply a delayed but accelerated IGM metal-enrichment scenario in the latter model as studied in Section 4 that follows.

4 THE IGM METAL ENRICHMENT IN CDM AND WDM AND COMPARISON WITH OBSERVATIONS

We now use the ejected gas mass density values, calculated above, to obtain an estimate of the IGM metal enrichment in the two metallicity scenarios adopted in this work: the first where the gas-phase metallicity $Z_{\rm gas} = 0.2\,{\rm Z}_{\odot}$ for all galaxies and the second where $Z_{\rm gas}$ for a given galaxy is computed depending on its stellar mass. Given that the C IV content, estimated from quasar absorption lines, is used as an indicator of the IGM metal enrichment ($\Omega_{\rm C\,IV}$), we convert our values of the gas mass density ejected by a galaxy into the C IV density parameter using $\Omega_{\rm C\,IV} = \rho_{\rm C\,IV}/\rho_{\rm c}$. Here $\rho_{\rm C\,IV}$ and $\rho_{\rm c}$ represent the C IV and critical densities, respectively. Further, $\rho_{\rm C\,IV}$ is calculated by summing over the gas mass ejected by all the, say N, galaxies at a given z such that

$$\rho_{\rm C\,IV} = \sum_{i=1}^{N} \rho_{\rm gas,ej}(i) \times Z_{\rm gas}(i) \times f({\rm C}/Z) \times f({\rm C\,IV}/{\rm C}), \qquad (1)$$

where for each galaxy (i) $\rho_{\rm gas,\,ej}(i)$ is the total gas mass density ejected by the galaxy over its lifetime till z and $Z_{\rm gas}$ is the metallicity of the perfectly mixed ISM gas. Further, $f({\rm C}/Z)$ is the fraction of metals in the form of carbon and $f({\rm C\,IV}/{\rm C})$ represents the fraction of triply ionized carbon. Assuming SNII to be the main dust sources, the value of $f({\rm C}/Z)$ is obtained by extrapolating the SNII yields (between 13 and 40 $\rm M_{\odot}$) given by Nomoto et al. (2006) down to 8 $\rm M_{\odot}$ and weighting these over a Salpeter IMF between 8 and 40 $\rm M_{\odot}$; stars with mass $\gtrsim 40\,{\rm M}_{\odot}$ collapse to black holes with little contribution to the metal budget. This calculation results in a value of $f({\rm C}/Z) \simeq 0.14$. We use the results from Keating et al. (2016) and García et al. (2017b) to find $\log({\rm C\,IV}/{\rm C}) = -0.35(z+1) + 1.45$ for $z \gtrsim 4$, yielding $f({\rm C\,IV}/{\rm C}) \simeq 0.5$ at $z = 4$, consistent with observations and photometric modelling by Simcoe (2011), that decreases to $f({\rm C\,IV}/{\rm C}) \simeq 0.009$ by $z = 9$. We note that in using the $f({\rm C}/Z)$ yield purely from SNII, we have neglected the metal contribution from metal-free (Pop III) stars. This is justified by the fact that observations of high-z UV slopes (Dunlop et al. 2013; Rogers, McLure & Dunlop 2013; Bouwens et al. 2014; Rogers et al. 2014; Oesch et al. 2016) and star formation clumps (Vanzella et al. 2017) show no indication of metal-free stellar populations, a result that is supported by theoretical simulations that find Pop III stars to contribute ≤ 10 per cent to star formation at $z \leq 7$–10 (Tornatore, Ferrara & Schneider 2007; Maio et al. 2010; Pallottini et al. 2014; Jaacks et al. 2018) and < 5 per cent to the luminosity for galaxies with $M_{\rm UV} < -16$ at $z = 10$ (Salvaterra, Ferrara & Dayal 2011). Furthermore, the observed ratios of C II, O I, Si II, and Fe II in quasar absorption line systems at $4.7 < z < 6.3$ show no differences with respect to metal-poor systems at lower redshifts (Becker et al. 2012).

We start with the simplest scenario where each galaxy has a fixed metallicity of $Z_{\rm gas} = 0.2\,{\rm Z}_{\odot}$. This assumption likely overestimates (underestimates) the metallicity values for low-mass galaxies at high z (high-mass galaxies at low z). The $\Omega_{\rm C\,IV}(z)$ values arising from these calculations for CDM, 1.5 and 3 keV WDM are shown in Fig. 5.

We focus on comparing our results, for CDM, 3 and 1.5 keV WDM, to the $\Omega_{\rm C\,IV}$ observational data at $z \simeq 5.5$ given that metal enrichment from asymptotic giant branch (AGB) stars, which we have neglected in our calculations, could have had a significant contribution at lower z; we note that we have used the same baryonic free parameter values for all three models. We find that the CDM and 3 keV WDM fiducial models where all galaxies contribute to the IGM metal enrichment agree with the observational data points of Simcoe et al. (2011) and Díaz et al. (2016, that supersedes Ryan-Weber et al. 2009). Within error bars, the Díaz et al. (2016) point, with the lowest measured $\Omega_{\rm C\,IV}$ value at $z \sim 5.5$, also matches the CDM model with complete UV suppression in galaxies with $v_{\rm circ} < 30\,{\rm km\,s^{-1}}$ as well as the fiducial 1.5 keV WDM model. The intermediate Simcoe et al. (2011) point rules out all models except fiducial CDM and 3 keV at $\gtrsim 1.6\sigma$. On the other hand, with its highest measured value of $\Omega_{\rm C\,IV}$ at $z \sim 5.5$, the D'Odorico et al. (2013) point only allows the CDM fiducial model, ruling out the 3 keV WDM fiducial model (all other models) at $\approx 1.1\sigma$ ($\gtrsim 1.5\sigma$).

As for the key metal polluters, our results show that, in the fiducial model, galaxies with $M_{\rm UV} \gtrsim -15$ ($M_{\rm UV} \lesssim -15$) could provide roughly 50 per cent (80 per cent) of the IGM metal budget in CDM (1.5 keV WDM) model by $z \simeq 4.5$. As expected, the currently detected brighter galaxies, with $M_{\rm UV} \lesssim -18$, have a smaller contribution of about 22 per cent (38 per cent) to the metal budget for CDM (1.5 keV WDM); the results from the 3 keV model naturally lie between CDM and 1.5 keV WDM.

Parametrizing the $\Omega_{\rm C\,IV}$–z relation as $\log(\Omega_{\rm C\,IV}) = a(1+z) + b$, we show the slopes for all CDM and 1.5 keV WDM models in Table 1. We start by noting that the steeper z-evolution of $\rho_{\rm gas,\,ej}$ in 1.5 keV WDM with respect to CDM is reflected in its steeper (by a factor of 1.3) $\Omega_{\rm C\,IV}$–z relation – the fiducial CDM model predicts a 27 times higher value of C IV compared to the fiducial 1.5 keV model

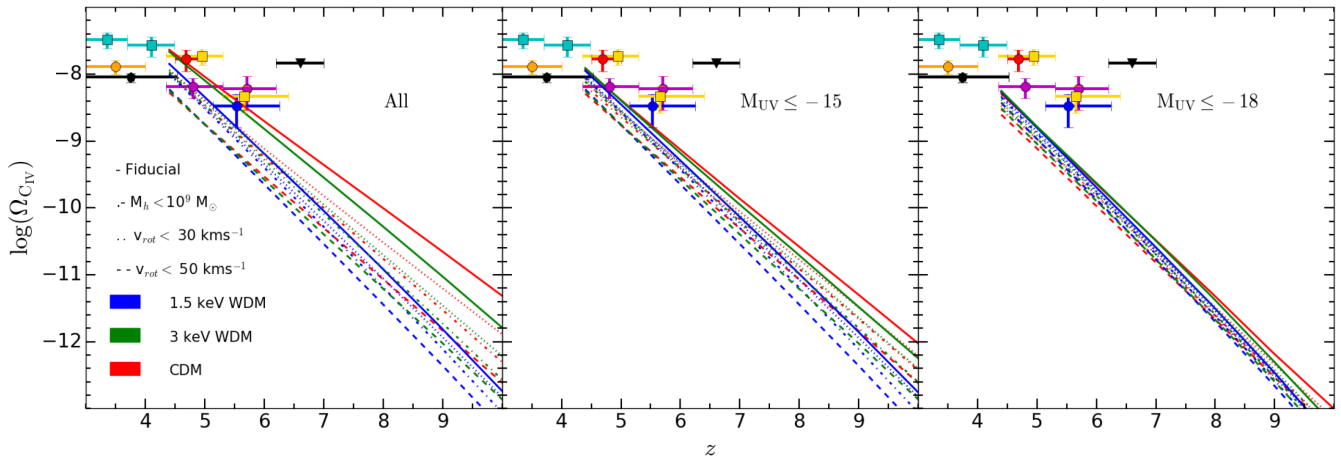

Figure 5. The cosmic mass density of C IV, $\Omega_{C\,IV}$, measured as a function of redshift assuming all galaxies to have $Z_{gas} = 0.2\,Z_\odot$, independent of mass and redshift, for all galaxies (left-hand panel), galaxies with $M_{UV} \lesssim -15$ (middle panel), and $M_{UV} \lesssim -18$ (right-hand panel). In each panel, the red, green, and blue lines show results for CDM, 3 keV WDM, and 1.5 keV WDM, respectively, for the different feedback models noted in the legend. Points indicate the C IV density parameter inferred observationally by Pettini et al. (2003, rescaled by Ryan-Weber et al. 2009, red circle), D'Odorico et al. (2010, orange circle), Simcoe et al. (2011, gold squares), Cooksey et al. (2013, black pentagon), D'Odorico et al. (2013, magenta circles), Boksenberg & Sargent (2015, cyan squares), Díaz et al. (2016, blue circle), and Bosman et al. (2017, black triangle showing upper limit).

Table 1. Parametrizing the $\Omega_{C\,IV}$–z relation as $\log(\Omega_{C\,IV}) = a(1+z) + b$, we show the slopes ($a$) for all CDM and 1.5 keV WDM models for the two cases considered in Section 4: the first where $Z_{gas} = 0.20\,Z_\odot$ and the second where $Z_{gas} = \mathrm{fn}(M_*)$.

DM model	Fiducial model	$M_h < 10^9\,M_\odot$	$v_c < 30\,km\,s^{-1}$	$v_c < 50\,km\,s^{-1}$
		Slopes (a) for $Z_{gas} = 0.20\,Z_\odot$		
CDM	−0.66	−0.77	−0.70	−0.77
1.5 keV WDM	−0.87	−0.90	−0.86	−0.90
		Slopes (a) for $Z_{gas} = \mathrm{fn}(M_*)$		
CDM	−0.66	−0.77	−0.71	−0.78
1.5 keV WDM	−0.88	−0.91	−0.87	−0.92

at $z \simeq 10$, reducing to a factor of about 2 by $z = 5$. Given the lack of low-mass haloes, the impact of UV feedback is naturally lesser on the 1.5 keV WDM model as compared to CDM, resulting in a larger steepening of CDM slopes. As shown in the same table, the CDM slopes are shallower by a factor of $a \sim 1.1$–1.2 when compared to 1.5 keV WDM.

While, as expected, the CDM fiducial model shows the highest value of $\Omega_{C\,IV}$, these results show a degeneracy between the underlying DM model and the baryonic feedback prescription implemented. This highlights the fact that an intrinsic dearth of low-mass haloes (in light WDM models) is equivalent to increasing the UV feedback, thereby suppressing the baryonic content and star formation capabilities of low-mass haloes in CDM. For example, at $z \simeq 5.5$–9, the 1.5 keV WDM fiducial model lies between the CDM models with UV suppression limits of $v_{circ} \lesssim 30$ and $v_{circ} \lesssim 50\,km\,s^{-1}$, analogous to the UV LF behaviour seen in Section 3.1.

In order to check the dependence of our results on the assumed metallicity, we explore an alternative scenario in which the gas-phase metallicity scales with the stellar mass. This assumption is motivated by the observed mass–metallicity relation (MZR) linking the gas-phase metallicity and stellar mass from $z = 0$ to ∼4 (Tremonti et al. 2004; Lee et al. 2006; Maiolino et al. 2008; Mannucci et al. 2009; Zahid et al. 2012; Hunt et al. 2016). For this work, we use the results, at the highest measured redshifts of $z = 3$–4, from the LSD and AMAZE surveys (Maiolino et al. 2008; Mannucci et al. 2009), which can be fitted to yield $\log(Z_{gas}/Z_\odot) = 0.383\log(M_*) - 4.307$ for galaxies with $M_* \gtrsim 10^{9.4}\,M_\odot$; we assume each galaxy to have $Z_{gas} = 0.20\,Z_\odot$ below this mass range.[1] We use equation (1) to recompute the value of $\Omega_{C\,IV}(z)$ using this M_*-dependent metallicity, the results of which are shown in Fig. 6 and in Table 1. Interestingly, we find these results to be indistinguishable, in terms of the $\Omega_{C\,IV}$ values, from those assuming a constant metallicity of $Z_{gas} = 0.20\,Z_\odot$: this is driven by the fact that low-mass galaxies, which are the key contributors to the ejected gas mass density as shown in Section 3.3, are assumed to have the same gas-phase metallicity in both the models considered here. However, the larger metallicities of massive galaxies in the latter calculation result in massive galaxies ($M_{UV} \lesssim -18$) having a larger contribution to the IGM metal budget: in the fiducial CDM (1.5 keV WDM) model, these galaxies contribute 28 per cent (46 per cent) to the IGM metal budget by $z \simeq 4.5$ as compared to the slightly lower values of 22 per cent (38 per cent) assuming a constant metallicity of $0.2\,Z_\odot$. Critically, we find that assuming an M_*-dependent

[1] Using a lower value of $Z_{gas} = 0.10\,Z_\odot$ results in all models underpredicting the $\Omega_{C\,IV}$ values as compared to observations at $z \gtrsim 4.5$. However, this result in not unreasonable given our assumption of metals being homogeneously distributed in the IGM.

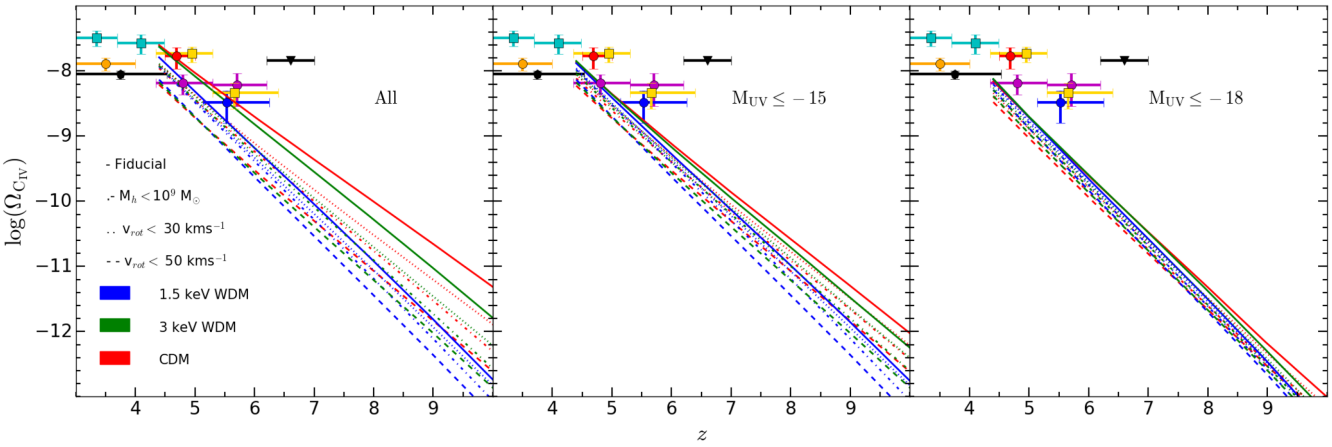

Figure 6. The cosmic mass density of C IV, $\Omega_{C\,IV}$, measured as a function of redshift assuming all galaxies to have $Z_{gas} = fn(M_*)$. Results are shown for all galaxies (left-hand panel), galaxies with $M_{UV} \lesssim -15$ (middle panel), and $M_{UV} \lesssim -18$ (right-hand panel). In each panel, the red and blue lines show results for CDM and 1.5 keV WDM, respectively, for the different feedback models noted in the legend. Points indicate observational data for which the references are shown in the caption of Fig. 5.

metallicity has no sensible impact on the $\Omega_{C\,IV}-z$ relation for any of the CDM or 1.5 keV WDM models or their relative differences, both including/excluding the impact of UV feedback.

We note that our calculations have involved a number of simplifications that are now summarized: (i) all metals are assumed to be perfectly mixed with gas implying outflows to have the same metallicity as the ISM gas; (ii) at any z, we assume at least the lowest mass galaxies ($M_* \lesssim 10^{9.4}\,M_\odot$) to have a fixed gas metallicity of $Z_{gas} = 0.2\,Z_\odot$, which is, most likely, an overestimation at the highest redshifts; (iii) we use a halo mass-independent C IV/C ratio to which the C IV density is sensitive; (iv) we have only considered carbon yields from SNII, neglecting the contribution from AGB stars that would have a significant impact, especially at $z \lesssim 5$ at which the metal mass would be underestimated; (v) while metals should be concentrated in overdense regions, we assume them to be homogeneously distributed over the IGM in order to infer the $\Omega_{C\,IV}$ value; and (vi) Z_{gas}, and in turn the extent to which the IGM is polluted with metals, critically depends on the metallicity of inflowing and outflowing gas: outflows preferentially carrying away metals can lead to an enhanced IGM metallicity enrichment whilst lowering the ISM metallicity. On the other hand, inflows of metal-poor gas can dilute the ISM metallicity whilst inflows of metal-enriched gas, possibly previously ejected by the galaxy (the so-called galactic fountain), can increase the ISM metallicity. Whilst assuming perfect mixing in this case results in a lower (higher) IGM metallicity in these two scenarios, respectively, relaxing this assumption can either enhance/decrease the IGM metallicity, depending on the metal richness (metal-to-gas ratio) of the outflows. However, accounting for such non-linear effects requires simultaneously, and consistently, modelling the metal cycle in the ISM and IGM, which, extending much beyond the scope of this proof-of-concept paper, is deferred to future works.

At this point, in addition to the metal cycle and baryon prescription-cosmology degeneracies discussed above, we highlight other key degeneracies that could lead to similar physical scenarios: first, the metallicity of outflowing gas has a degeneracy with the fractional volume of the IGM polluted with metals, i.e. a given value of the IGM metallicity can be obtained by polluting a small (large) fraction of the IGM with low (high) metallicity gas. However, this calculation is extremely hard to carry out without modelling both the metal enrichment and metal dispersion calculations in the IGM. Furthermore, it must be noted that the 'average' value of the IGM metallicity is hard to obtain observationally given it is only measured along a few lines of sight. A second degeneracy that can arise in such calculations is cosmology dependent: given that CDM collapses on all scales, the clumping factor (overdensity above average) of the IGM is expected to be higher than for WDM where low-σ density fluctuations can get wiped out. Reasonably assuming metal pollution to percolate more easily in low-density regions, this implies that the IGM in CDM could have a lesser volume (of denser gas) metal enriched to a higher level than WDM assuming the same amount of metals ejected into the IGM. However, this patchy metal enrichment could possibly be countered by the more homogeneous galaxy distribution in CDM as opposed to the larger galaxy bias expected in WDM. However, such calculations require, both, spatial information of galaxy positions as well as jointly tracking the baryonic assembly and metal exchange between the ISM and IGM that we defer to future works.

5 CONCLUSIONS AND DISCUSSION

This *proof-of-concept* work focuses on studying the metal enrichment of the IGM in CDM and WDM (1.5 keV) cosmologies using DELPHI – a semi-analytic model (Dayal et al. 2014, 2015, 2017a,b) that jointly tracks the DM and baryonic assembly of high-redshift ($z \gtrsim 4$) galaxies. This work is motivated by the fact that, compared to CDM, 1.5 keV WDM has a significant fraction ($\gtrsim 95$ per cent) of bound DM mass missing in low-mass haloes ($M_h \lesssim 10^{9.5}\,M_\odot$) at any cosmic epoch – this loss of shallow potential wells, expected to be the key IGM metal polluters, would naturally result in a delayed and lower metal enrichment in 1.5 keV WDM when compared to CDM. In addition to the *fiducial* (SNII feedback only) model, we explore three 'maximal' scenarios for reionization feedback by completely suppressing the gas mass, and hence star formation capabilities, in all haloes below: (i) $M_h = 10^9\,M_\odot$; (ii) $v_{circ} = 30\,km\,s^{-1}$; and (iii) $v_{circ} = 50\,km\,s^{-1}$. The model uses two mass- and z-independent free parameters – the fraction of SNII energy coupling to the gas (f_w) and the instantaneous star formation efficiency (f_*) to capture the key physics driving early galaxies. These are calibrated to the observed UV LF at $z \simeq 5$–10 yielding $f_w = 10$ per cent and $f_* = 3.5$ per cent for the fiducial model, and we use the same parameter values for all models.

We find that while the latest LBG UV LFs (Bouwens et al. 2017; Livermore et al. 2017) are consistent with CDM and the 3 and 1.5 keV fiducial (SNII feedback only) models, they allow ruling out maximal UV feedback suppression below $v_{\rm circ} = 50\,{\rm km\,s^{-1}}$ for CDM and *all maximal* UV feedback models for 1.5 keV WDM. However, given that it is only measured for massive $M_{\rm UV} \lesssim -18$ galaxies, as of now, all models are compatible with the SMD – as noted in previous works, the SMD will have to be measured down to magnitudes as faint as $M_{\rm UV} = -16.5$, with e.g. the *JWST*, to be able to distinguish between CDM and 1.5 keV WDM (e.g. Dayal et al. 2014). In terms of the total ejected gas mass density, we find that while galaxies fainter than $M_{\rm UV} = -15$ contribute most (∼55 per cent) to this quantity in CDM at $z = 5$, the trend reverses with $M_{\rm UV} \lesssim -15$ galaxies dominating in 1.5 keV WDM.

We explore two gas-phase metallicity scenarios: one where all galaxies have a constant gas-phase metallicity of $Z_{\rm gas} = 0.2\,{\rm Z_\odot}$ and the other in which we assign metallicities using the $z \sim 3$–4 MZR for galaxies with $M_* \gtrsim 10^{9.4}\,{\rm M_\odot}$ with lower mass galaxies assumed to have a fixed metallicity of $Z_{\rm gas} = 0.2\,{\rm Z_\odot}$. Assuming all galaxies to have a constant gas-phase metallicity of $Z_{\rm gas} = 0.2\,{\rm Z_\odot}$, a natural consequence is that $M_{\rm UV} \gtrsim -15$ ($M_{\rm UV} \lesssim -15$) galaxies are the key IGM metal polluters in CDM (1.5 keV WDM), contributing ∼50 per cent (80 per cent) to the total IGM metal budget at $z \simeq 4.5$ with currently detected galaxies ($M_{\rm UV} \lesssim -18$) contributing ∼22 per cent (38 per cent) to the IGM metal budget; applying the MZR observed at the highest redshifts of $z \sim 3$–4 yields qualitatively similar results, with the metal contribution from observed galaxies increasing slightly to 28 per cent (46 per cent) in the fiducial CDM (1.5 keV WDM) model.

Independent of the two gas-phase metallicity models assumed in this work, current observations on the IGM metal budget, obtained through measurements of $\Omega_{\rm C\,IV}$, especially at $z \sim 5.5$, allow the following constraints: while, within its 1σ error bars, the Díaz et al. (2016) point is consistent with both the fiducial and maximal reionization feedback (suppressing all haloes below $v_{\rm circ} = 30\,{\rm km\,s^{-1}}$) models for CDM and the 3 and 1.5 keV WDM fiducial models, the Simcoe et al. (2011) point rules out all models except fiducial CDM and 3 keV at $>1.6\sigma$. Our results therefore imply that, combining the two different data sets provided by the evolving UV LF and IGM metal density (Simcoe et al. 2011; D'Odorico et al. 2013), we can effectively rule out all models other than fiducial CDM; a combination of the UV LF and the Díaz et al. (2016) points provides a weaker constraint, allowing fiducial CDM and the 3 and 1.5 keV WDM models, as well as CDM with UV suppression of all haloes with $v_{\rm circ} \lesssim 30\,{\rm km\,s^{-1}}$. Tightening the error bars on $\Omega_{\rm C\,IV}$, future observations at $z \gtrsim 5.5$ could therefore well allow ruling out WDM as light as 1.5 keV.

ACKNOWLEDGEMENTS

JB and PD acknowledge support from the European Research Council's starting grant ERC StG-717001 'DELPHI'. PD acknowledges support from the European Commission's and University of Groningen's CO-FUND Rosalind Franklin programme. ERW acknowledges the support of Australian Research Council grant DP1095600.

REFERENCES

Atek H. et al., 2015, ApJ, 814, 69
Baur J., Palanque-Delabrouille N., Yèche C., Magneville C., Viel M., 2016, J. Cosmol. Astropart. Phys., 8, 012
Becker G. D., Sargent W. L. W., Rauch M., Carswell R. F., 2012, ApJ, 744, 91
Benson A. J. et al., 2013, MNRAS, 428, 1774
Birrer S., Amara A., Refregier A., 2017, J. Cosmol. Astropart. Phys., 5, 037
Bode P., Ostriker J. P., Turok N., 2001, ApJ, 556, 93
Boksenberg A., Sargent W. L. W., 2015, ApJS, 218, 7
Bosman S. E. I., Becker G. D., Haehnelt M. G., Hewett P. C., McMahon R. G., Mortlock D. J., Simpson C., Venemans B. P., 2017, MNRAS, 470, 1919
Bouwens R. J. et al., 2010, ApJ, 725, 1587
Bouwens R. J. et al., 2011, ApJ, 737, 90
Bouwens R. J. et al., 2014, ApJ, 793, 115
Bouwens R. J. et al., 2015, ApJ, 803, 34
Bouwens R. J. et al., 2016, ApJ, 830, 67
Bouwens R. J., Oesch P. A., Illingworth G. D., Ellis R. S., Stefanon M., 2017, ApJ, 843, 129
Bowler R. A. A. et al., 2014, MNRAS, 440, 2810
Bowler R. A. A. et al., 2015, MNRAS, 452, 1817
Boyarsky A., Ruchayskiy O., Iakubovskyi D., Franse J., 2014, Phys. Rev. Lett., 113, 251301
Boylan-Kolchin M., Bullock J. S., Kaplinghat M., 2011, MNRAS, 415, L40
Boylan-Kolchin M., Bullock J. S., Kaplinghat M., 2012, MNRAS, 422, 1203
Bradley L. D. et al., 2012, ApJ, 760, 108
Bulbul E., Markevitch M., Foster A., Smith R. K., Loewenstein M., Randall S. W., 2014, ApJ, 789, 13
Cappelluti N. et al., 2018, ApJ, 854, 179
Castellano M. et al., 2010, A&A, 524, A28
Cooksey K. L., Kao M. M., Simcoe R. A., O'Meara J. M., Prochaska J. X., 2013, ApJ, 763, 37
D'Odorico V., Calura F., Cristiani S., Viel M., 2010, MNRAS, 401, 2715
D'Odorico V. et al., 2013, MNRAS, 435, 1198
Dayal P., Ferrara A., Dunlop J. S., Pacucci F., 2014, MNRAS, 445, 2545
Dayal P., Mesinger A., Pacucci F., 2015, ApJ, 806, 67
Dayal P., Choudhury T. R., Bromm V., Pacucci F., 2017a, ApJ, 836, 16
Dayal P., Choudhury T. R., Pacucci F., Bromm V., 2017b, MNRAS, 472, 4414
de Souza R. S., Mesinger A., Ferrara A., Haiman Z., Perna R., Yoshida N., 2013, MNRAS, 432, 3218
Del Popolo A., Le Delliou M., 2014, J. Cosmol. Astropart. Phys., 12, 051
Del Popolo A., Le Delliou M., 2017, Galaxies, 5, 17
Di Cintio A., Brook C. B., Dutton A. A., Macciò A. V., Stinson G. S., Knebe A., 2014, MNRAS, 441, 2986
Díaz C. G., Ryan-Weber E. V., Cooke J., Koyama Y., Ouchi M., 2015, MNRAS, 448, 1240
Díaz C. G., Ryan-Weber E. V., Codoreanu A., Pettini M., Madau P., 2016, Bol. Asociacion Argentina Astron., 58, 54
Du X., Behrens C., Niemeyer J. C., 2017, MNRAS, 465, 941
Duncan K. et al., 2014, MNRAS, 444, 2960
Dunlop J. S. et al., 2013, MNRAS, 432, 3520
Finlator K., Thompson R., Huang S., Davé R., Zackrisson E., Oppenheimer B. D., 2015, MNRAS, 447, 2526
García L. A., Tescari E., Ryan-Weber E. V., Wyithe J. S. B., 2017a, MNRAS, 469, L53
García L. A., Tescari E., Ryan-Weber E. V., Wyithe J. S. B., 2017b, MNRAS, 470, 2494
Garrison-Kimmel S., Rocha M., Boylan-Kolchin M., Bullock J. S., Lally J., 2013, MNRAS, 433, 3539
González V., Labbé I., Bouwens R. J., Illingworth G., Franx M., Kriek M., 2011, ApJ, 735, L34
Governato F. et al., 2012, MNRAS, 422, 1231
Governato F. et al., 2015, MNRAS, 448, 792
Grazian A. et al., 2015, A&A, 575, A96
Hu W., Barkana R., Gruzinov A., 2000, Phys. Rev. Lett., 85, 1158
Hui L., Ostriker J. P., Tremaine S., Witten E., 2017, Phys. Rev. D, 95, 043541

Hunt L., Dayal P., Magrini L., Ferrara A., 2016, MNRAS, 463, 2002
Inoue K. T., Takahashi R., Takahashi T., Ishiyama T., 2015, MNRAS, 448, 2704
Iršič V. et al., 2017, Phys. Rev. D, 96, 023522
Ishigaki M., Kawamata R., Ouchi M., Oguri M., Shimasaku K., Ono Y., 2018, ApJ, 854, 73
Jaacks J., Thompson R., Finkelstein S. L., Bromm V., 2018, MNRAS, 475, 4396
Jethwa P., Erkal D., Belokurov V., 2018, MNRAS, 473, 2060
Keating L. C., Puchwein E., Haehnelt M. G., Bird S., Bolton J. S., 2016, MNRAS, 461, 606
Kennedy R., Frenk C., Cole S., Benson A., 2014, MNRAS, 442, 2487
Klypin A., Kravtsov A. V., Valenzuela O., Prada F., 1999, ApJ, 522, 82
Koposov S. E., Yoo J., Rix H.-W., Weinberg D. H., Macciò A. V., Escudé J. M., 2009, ApJ, 696, 2179
Labbé I. et al., 2010a, ApJ, 708, L26
Labbé I. et al., 2010b, ApJ, 716, L103
Labbé I. et al., 2013, ApJ, 777, L19
Lee H., Skillman E. D., Cannon J. M., Jackson D. C., Gehrz R. D., Polomski E. F., Woodward C. E., 2006, ApJ, 647, 970
Lee K.-S. et al., 2012, ApJ, 752, 66
Leitherer C. et al., 1999, ApJS, 123, 3
Leitherer C., Ortiz Otálvaro P. A., Bresolin F., Kudritzki R.-P., Lo Faro B., Pauldrach A. W. A., Pettini M., Rix S. A., 2010, ApJS, 189, 309
Livermore R. C., Finkelstein S. L., Lotz J. M., 2017, ApJ, 835, 113
Lopez-Honorez L., Mena O., Palomares-Ruiz S., Villanueva-Domingo P., 2017, Phys. Rev. D, 96, 103539
Macciò A. V., Stinson G., Brook C. B., Wadsley J., Couchman H. M. P., Shen S., Gibson B. K., Quinn T., 2012a, ApJ, 744, L9
Macciò A. V., Paduroiu S., Anderhalden D., Schneider A., Moore B., 2012b, MNRAS, 424, 1105
McLeod D. J., McLure R. J., Dunlop J. S., 2016, MNRAS, 459, 3812
McLure R. J., Dunlop J. S., Cirasuolo M., Koekemoer A. M., Sabbi E., Stark D. P., Targett T. A., Ellis R. S., 2010, MNRAS, 403, 960
McLure R. J. et al., 2013, MNRAS, 432, 2696
Madau P., Shen S., Governato F., 2014, ApJ, 789, L17
Maio U., Ciardi B., Dolag K., Tornatore L., Khochfar S., 2010, MNRAS, 407, 1003
Maiolino R. et al., 2008, A&A, 488, 463
Mannucci F. et al., 2009, MNRAS, 398, 1915
Menci N., Sanchez N. G., Castellano M., Grazian A., 2016a, ApJ, 818, 90
Menci N., Grazian A., Castellano M., Sanchez N. G., 2016b, ApJ, 825, L1
Moore B., Ghigna S., Governato F., Lake G., Quinn T., Stadel J., Tozzi P., 1999a, ApJ, 524, L19
Moore B., Quinn T., Governato F., Stadel J., Lake G., 1999b, MNRAS, 310, 1147
Navarro J. F., Frenk C. S., White S. D. M., 1997, ApJ, 490, 493
Nomoto K., Tominaga N., Umeda H., Kobayashi C., Maeda K., 2006, Nucl. Phys. A, 777, 424
Ocvirk P. et al., 2016, MNRAS, 463, 1462
Oesch P. A. et al., 2010, ApJ, 709, L16
Oesch P. A. et al., 2013, ApJ, 773, 75
Oesch P. A. et al., 2014, ApJ, 786, 108
Oesch P. A. et al., 2016, ApJ, 819, 129
Okamoto T., Gao L., Theuns T., 2008, MNRAS, 390, 920
Oppenheimer B. D., Davé R., Finlator K., 2009, MNRAS, 396, 729
Pacucci F., Mesinger A., Haiman Z., 2013, MNRAS, 435, L53
Pallottini A., Ferrara A., Gallerani S., Salvadori S., D'Odorico V., 2014, MNRAS, 440, 2498
Parkinson H., Cole S., Helly J., 2008, MNRAS, 383, 557
Peñarrubia J., Pontzen A., Walker M. G., Koposov S. E., 2012, ApJ, 759, L42
Petkova M., Springel V., 2011, MNRAS, 412, 935
Pettini M., Madau P., Bolte M., Prochaska J. X., Ellison S. L., Fan X., 2003, ApJ, 594, 695
Planck C ollaboration XIII, 2016, A&A, 594, A13
Rocha M., Peter A. H. G., Bullock J. S., Kaplinghat M., Garrison-Kimmel S., Oñorbe J., Moustakas L. A., 2013, MNRAS, 430, 81
Rogers A. B., McLure R. J., Dunlop J. S., 2013, MNRAS, 429, 2456
Rogers A. B. et al., 2014, MNRAS, 440, 3714
Ryan-Weber E. V., Pettini M., Madau P., Zych B. J., 2009, MNRAS, 395, 1476
Salpeter E. E., 1955, ApJ, 121, 161
Salvaterra R., Ferrara A., Dayal P., 2011, MNRAS, 414, 847
Schneider A., Anderhalden D., Macciò A. V., Diemand J., 2014, MNRAS, 441, L6
Shen S., Madau P., Guedes J., Mayer L., Prochaska J. X., Wadsley J., 2013, ApJ, 765, 89
Silk J., 2017, ApJ, 839, L13
Simcoe R. A., 2011, ApJ, 738, 159
Simcoe R. A. et al., 2011, ApJ, 743, 21
Song M. et al., 2016, ApJ, 825, 5
Spergel D. N., Steinhardt P. J., 2000, Phys. Rev. Lett., 84, 3760
Stark D. P., Schenker M. A., Ellis R., Robertson B., McLure R., Dunlop J., 2013, ApJ, 763, 129
Tan W.-W., Wang F. Y., Cheng K. S., 2016, ApJ, 829, 29
Tornatore L., Ferrara A., Schneider R., 2007, MNRAS, 382, 945
Tremonti C. A. et al., 2004, ApJ, 613, 898
Vanzella E. et al., 2017, MNRAS, 467, 4304
Viel M., Lesgourgues J., Haehnelt M. G., Matarrese S., Riotto A., 2005, Phys. Rev. D, 71, 063534
Viel M., Becker G. D., Bolton J. S., Haehnelt M. G., 2013, Phys. Rev. D, 88, 043502
Vogelsberger M., Zavala J., Simpson C., Jenkins A., 2014, MNRAS, 444, 3684
Wang M.-Y., Peter A. H. G., Strigari L. E., Zentner A. R., Arant B., Garrison-Kimmel S., Rocha M., 2014, MNRAS, 445, 614
Weinberg D. H., Bullock J. S., Governato F., Kuzio de Naray R., Peter A. H. G., 2015, Proc. Natl. Acad. Sci., 112, 12249
Yabe K., Ohta K., Iwata I., Sawicki M., Tamura N., Akiyama M., Aoki K., 2009, ApJ, 693, 507
Zahid H. J., Bresolin F., Kewley L. J., Coil A. L., Davé R., 2012, ApJ, 750, 120

This paper has been typeset from a TEX/LATEX file prepared by the author.